Study on Two-Coil and Four-Coil Wireless Power Transfer Systems Using Z-Parameter Approach

Dong-Wook Seo, Jae-Ho Lee, and Hyung Soo Lee

A wireless power transfer (WPT) system is usually classified as being of either a two-coil or four-coil type. It is known that two-coil WPT systems are suitable for short-range transmissions, whereas four-coil WPT systems are suitable for mid-range transmissions. However, this paper reveals that the two aforementioned types of WPT system are alike in terms of their performance and characteristics, differing only when it comes to their matching-network configurations. In this paper, we first find the optimum load and source conditions using Z-parameters. Then, we estimate the maximum power transfer efficiency under the optimum load and source conditions, and we describe how to configure the matching networks pertaining to both types of WPT system for the given optimum load and source conditions. The two types of WPT system show the same performance with respect to the coupling coefficient and load impedance. Further, they also demonstrate an identical performance in the two cases considered in this paper, that is, a strong-coupled case and a weak-coupled case.

Keywords: Four-coil wireless power transfer system, matching network, power gain, power transfer efficiency, transducer power gain, two-coil wireless power transfer system, two-port network, Z-parameter.

I. Introduction

In 2007, using coupled mode theory, Soljačić showed that a wireless power transmission is theoretically possible. The author demonstrated experimentally that a 60 W lightbulb could be lit by a 9.9 MHz source at a distance of 2 m [1], [2]. Since the publication of the results from [1] and [2], research related to wireless power transfer (WPT) has been on the rise.

A variety of methods such as the use of equivalent circuit models [3]–[8] and spherical mode theory [9] have been used to analyze WPT systems. The main points of concern regarding a WPT system are that of the maximum power transfer efficiency (PTE) and optimum load.

Since the 1970s, there have been numerous studies related to inductive coupling, whereby researchers have attempted to realize WPT or biotelemetry in implant devices. [10]–[13]. In the past, in the field of biomedical engineering, research has tended to predominantly focus on ways in which to transfer low power to implant devices; however, recently, attention has turned to focus upon ways in which to transfer high power (of up to several kilowatts) to various devices. Furthermore, early research tended to involve the use of two self-resonant coils, a primary coil and a secondary coil, in a WPT system. Soljačić, in contrast, used a four-coil system, adding source and load coils to the two aforementioned types of coil, and now standard, self-resonant coils [1].

Two- and four-coil WPT systems have different topologies and are known by alternative names; for example, in the case of a two-coil WPT system, we have "inductive coupled WPT" or "inductively coupled power transfer" or "inductive WPT," and in the case of a four-coil WPT system, we have "resonant coupled WPT" or "resonant WPT." Additionally, the authors of [14] through [16] claimed that two-coil WPT systems are

Manuscript received July 30, 2015; revised Jan. 26, 2016; accepted Feb. 18, 2016.

The research was supported by the Ministry of Science, ICT and Future Planning Through the Development for IT·SW industrial convergence original technology (ID: R0101-15-0147).

Dong-Wook Seo (seodongwook@etri.re.kr), Jae-Ho Lee (corresponding author, jhlee1229@etri.re.kr), and Hyung Soo Lee (hsulee@etri.re.kr) are with the Daegu-Gyeongbuk Research Center, ETRI, Daegu, Rep. of Korea.

suitable for only short-range transmissions and that four-coil WPT systems are suitable for only mid-range transmissions. However, in [14] and [15], it was shown that there is no guarantee that both a two-coil WPT system and a four-coil WPT system will operate with identical primary and secondary coils, because the inductance of either a two-coil, three-coil, or four-coil WPT system can be varied through an optimization process. Therefore, it is impossible to confirm whether any two such systems are designed to maximize the PTE at the same coupling coefficient.

In [16], as the coupling coefficient decreases, the real part of the input impedance for a two-coil WPT system was shown to decrease, whereas that of a four-coil WPT system was shown to contrarily increase. In [16], the authors insisted that these trends give rise to different suitable transmission distances for two-coil and four-coil WPT systems; however, their explanation is unfortunately oblique for readers to clearly understand the relation between the real part of the input impedance and the transmission distance. In addition, performance indexes such as the PTE and output power are not given either experimentally or through simulation.

In [17]–[20], source and load coils were introduced as impedance matching networks in a four-coil WPT system. However, the authors did not concretely represent the structures of such networks, instead only describing a simple concept of a matching network and comparison with the experiments in [1]. That is, the way in which the matching networks operate and are configured was not explained in any detail.

In this paper, we derive the optimum load and source conditions for the maximum PTE using the Z-parameters of a two-port network. Furthermore, we address whether a two-coil WPT system achieves a performance identical to that of a four-coil WPT system.

The remainder of this paper is organized as follows. In Section II, we assume a conventional two-coil WPT system as a two-port network, and derive both the operating power gain and transducer power gain using the two-port network's Z-parameters. We define the PTE as the transducer power gain, and derive the optimum load and source conditions as a simple closed-form expression for the ideal maximum PTE. The optimum load and source conditions are implemented using a matching network. In Section III, we deal with how to configure the matching networks of both a two-coil WPT system and a four-coil WPT system. Section IV shows that a two-coil and four-coil WPT system achieve the same performance when designed to maximize the PTE at the same coupling coefficient. In addition, we provide several case studies on two-coil and four-coil WPT systems. Finally, this paper ends with Section V, which contains some concluding remarks and a summary of the present work.

II. System Analysis

Figure 1(a) shows the equivalent circuit model of a two-coil series-resonant WPT system with voltage source V_s and arbitrary source and load impedances Z_s and Z_L. With the exclusion of the source and load parts, the rest of the system is represented as a two-port network (see Fig. 1(b)). The properties of the two-port network can be expressed in terms of the network parameters, such as *Z*, *Y*, *S*, and *ABCD* [21]. Because the inductive link is generally reciprocal, a two-coil series-resonant WPT system can be represented by a T-equivalent circuit having Z-parameters, as shown in Fig. 1(c).

From the definition of the [Z] matrix, the Z-parameters of the inductive link and series capacitors can be found as follows:

$$Z_{11} = \left.\frac{V_1}{I_1}\right|_{I_2=0} = R_1 + j\omega L_1 + \frac{1}{j\omega C_1}, \quad (1)$$

$$Z_{22} = \left.\frac{V_2}{I_2}\right|_{I_1=0} = R_2 + j\omega L_2 + \frac{1}{j\omega C_2}, \quad (2)$$

$$Z_{12} = \left.\frac{V_1}{I_2}\right|_{I_1=0} = j\omega M, \quad (3)$$

$$Z_{21} = \left.\frac{V_1}{I_1}\right|_{I_2=0} = j\omega M, \quad (4)$$

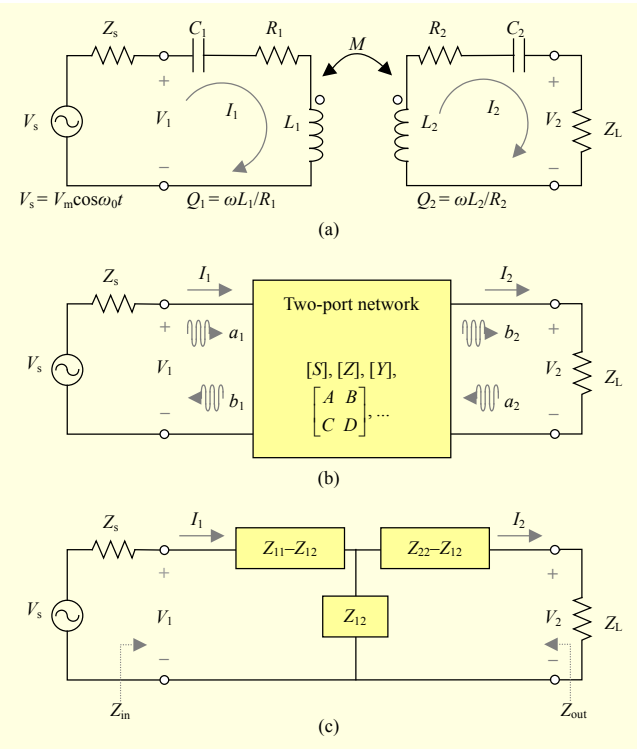

Fig. 1. Equivalent circuit model: (a) two-coil WPT system, (b) general two-port network, and (c) T-equivalent two-port network using Z-parameters.

where ω is an angular frequency, and V_1, V_2, I_1, and I_2 are the total voltage and current at the first and second ports, respectively. The variables R_1, L_1, R_2, and L_2 are the parasitic resistance and inductance of the primary and secondary coils, respectively; M is the mutual inductance between the primary and secondary coils.

For the T-equivalent two-port network of Fig. 1(c), the input impedance looking into the terminated two-port network from the generator end is

$$Z_{\text{in}} = Z_{11} - \frac{Z_{12}^2}{Z_{22} + Z_{\text{L}}}. \tag{5}$$

Similarly, the output impedance can be expressed as

$$Z_{\text{out}} = Z_{22} - \frac{Z_{12}^2}{Z_{11} + Z_{\text{s}}}. \tag{6}$$

1. Power Transfer Efficiency (PTE)

We now consider the PTE of a two-port network with an arbitrary source and load impedances. First, the power delivered to the input of the terminated two-port network is computed as

$$P_{\text{in}} = \frac{1}{2}|I_1|^2 \,\text{Re}\{Z_{\text{in}}\}, \tag{7}$$

where P_{in} is not the total power delivered by the source, but is the power delivered into the network. On the other hand, the power actually delivered to the load is given by

$$P_{\text{L}} = \frac{1}{2}|I_2|^2 \,\text{Re}\{Z_{\text{L}}\}. \tag{8}$$

The power gain can then be expressed as

$$G_{\text{p}} = \frac{P_{\text{L}}}{P_{\text{in}}} = \left|\frac{I_2}{I_1}\right|^2 \frac{\text{Re}\{Z_{\text{L}}\}}{\text{Re}\{Z_{\text{in}}\}} = \left|\frac{Z_{12}}{Z_{22} + Z_{\text{L}}}\right|^2 \frac{\text{Re}\{Z_{\text{L}}\}}{\text{Re}\{Z_{\text{in}}\}}. \tag{9}$$

The power gain of (9), also called the operating power gain, is the ratio of power dissipated in the load to the power delivered to the input of the network [21]. This gain is then independent of the source impedance Z_{s}, and dependent only on the load impedance Z_{L}. If the network delivers the maximum power to the load, then the operating power gain becomes the ideal maximum PTE. Because the operating power gain does not include the effect of the source impedance, it is incorrect for the PTE to be estimated from the operating power gain of (9), as shown in [22] and [23].

Of the several definitions of the power gain, on the other hand, the transducer power gain is well known to be the most useful for a terminated two-port network with an input source. The transducer power gain is defined as the ratio of the power delivered to the load to the power available from the source, and depends on the load impedance as well as the source impedance. The transducer power gain, G_{T}, is given by

$$G_{\text{T}} = \frac{P_{\text{L}}}{P_{\text{avs}}} = \frac{P_{\text{L}}}{P_{\text{in}}\big|_{\Gamma_{\text{in}} = \Gamma_{\text{s}}^* (\text{or } Z_{\text{in}} = Z_{\text{s}}^*)}}, \tag{10}$$

where P_{avs} represents the available power of the source, and becomes equal to P_{in} when the network is conjugate-matched to the source; that is, $P_{\text{in}} = P_{\text{avs}}$ when $Z_{\text{in}} = Z_{\text{s}}^*$ [21]. The power available from the source can then be regarded as the total power delivered by the input source (including the source impedance). Therefore, the PTE of a WPT system should be estimated by the transducer power gain.

Using Thevenin's theorem, we can find the relations between $I_2 = V_2/(Z_{\text{out}} + Z_{\text{s}})$ and $V_2 = V_{\text{s}}/(Z_{11} + Z_{\text{s}})$. Therefore, the power delivered to the load of (8) can be written in the following alternative form:

$$\begin{aligned} P_{\text{L}} &= \frac{1}{2}\left|\frac{V_2}{Z_{\text{out}} + Z_{\text{L}}}\right|^2 \text{Re}\{Z_{\text{L}}\} \\ &= \frac{1}{2}\frac{1}{|Z_{\text{out}} + Z_{\text{L}}|^2}\left|V_{\text{s}} \cdot \frac{Z_{12}}{Z_{11} + Z_{\text{s}}}\right|^2 \text{Re}\{Z_{\text{L}}\}. \end{aligned} \tag{11}$$

Similarly, (7) can be written as

$$P_{\text{in}} = \frac{1}{2}\left|\frac{V_{\text{s}}}{Z_{\text{in}} + Z_{\text{s}}}\right|^2 \text{Re}\{Z_{\text{in}}\}. \tag{12}$$

The power available from the source is obtained from (12) by setting $Z_{\text{in}} = Z_{\text{s}}^*$, and can then be written as

$$P_{\text{avs}} = \frac{1}{8}\frac{|V_{\text{s}}|^2}{\text{Re}\{Z_{\text{in}}\}}. \tag{13}$$

Substituting (11) and (13) into (10), the transducer power gain of a two-port network (that is, the PTE of a WPT system) is obtained in terms of the Z-parameters as follows:

$$G_{\text{T}} = \frac{4\,\text{Re}\{Z_{\text{s}}\}\,\text{Re}\{Z_{\text{L}}\}|Z_{21}|^2}{\left|(Z_{11} + Z_{\text{s}})(Z_{\text{out}} + Z_{\text{L}})\right|^2}. \tag{14}$$

2. Optimum Load, Optimum Source, and Maximum PTE

As mentioned previously, the operating power gain is not dependent on the source impedance, but only on the load impedance. Therefore, the operating power gain becomes the ideal maximum PTE when the network delivers the input power to the load. Consequently, we can find the optimum load condition to maximize the operating power gain. This optimum load condition is one of the requirements to achieving the ideal maximum PTE.

Actually, it is perfectly clear that the optimum load condition

ETRI Journal, Volume 38, Number 3, June 2016
http://dx.doi.org/10.4218/etrij.16.0115.0692

is obtained from the transducer power gain because the transducer power gain is considered as the PTE of a WPT system. However, it is cumbersome to obtain the optimum load from the transducer power gain, because the transducer power gain contains the effect of both the load and the source. We use the operating power gain with a relatively simple formula to derive the optimum load condition.

The substitution of (1) through (3) into (5) yields the following:

$$\mathrm{Re}\{Z_{\mathrm{in}}\} = R_1 + \frac{\omega^2 M^2 \left(R_2 + R_{\mathrm{L}}\right)}{\left(R_2 + R_{\mathrm{L}}\right)^2 + \left(\omega L_2 - \frac{1}{\omega C_2} + X_{\mathrm{L}}\right)^2}, \quad (15)$$

$$\mathrm{Im}\{Z_{\mathrm{in}}\} = \left(\omega L_1 - \frac{1}{\omega C_1}\right) - \frac{\omega^2 M^2 \left(\omega L_2 - \frac{1}{\omega C_2} + X_{\mathrm{L}}\right)}{\left(R_2 + R_{\mathrm{L}}\right)^2 + \left(\omega L_2 - \frac{1}{\omega C_2} + X_{\mathrm{L}}\right)^2}. \quad (16)$$

Using (2), (3), and (15), the operating power gain can be rewritten as

$$G_{\mathrm{p}} = \frac{\omega^2 M^2 R_{\mathrm{L}}}{\left[\left(R_2 + R_{\mathrm{L}}\right)^2 + \left(\omega L_2 - \frac{1}{\omega C_2} + X_{\mathrm{L}}\right)^2\right] \cdot R_1 + \omega^2 M^2 \left(R_2 + R_{\mathrm{L}}\right)}. \quad (17)$$

The reactance and resistance of the load impedance maximizing the operating power gain are

$$\frac{\partial G_{\mathrm{p}}}{\partial X_{\mathrm{L}}} = 0 \rightarrow X_{\mathrm{L,opt}} = -\left(\omega L_2 - \frac{1}{\omega C_2}\right), \quad (18)$$

$$\frac{\partial G_{\mathrm{p}}\big|_{X_{\mathrm{L}} = X_{\mathrm{L,opt}}}}{\partial R_{\mathrm{L}}} = 0 \rightarrow R_{\mathrm{L,opt}} = R_2\sqrt{1 + \frac{\omega^2 M^2}{R_1 R_2}} = R_2\sqrt{1 + k^2 Q_1 Q_2}, \quad (19)$$

where k is the coupling coefficient, and the relation between k and mutual inductance M is expressed as $M = k\sqrt{L_1 L_2}$. Equations (18) and (19) represent the optimum load condition. Therefore, the ideal maximum PTE is obtained by applying the optimum load condition to the operating power gain as follows:

$$\eta_{\max} = \left.\frac{\Delta}{\left(1 + \sqrt{1 + \Delta}\right)^2}\right|_{\Delta = k^2 Q_1 Q_2}, \quad (20)$$

where Δ is the figure of merit (FoM) of a WPT system, and a larger Δ guarantees a higher efficiency. Equation (20) is equal to the ideal maximum PTE in [11], [17], and [24].

Substituting (18) and (19) into (15) and (16), the input impedance of a WPT system with the optimum load is

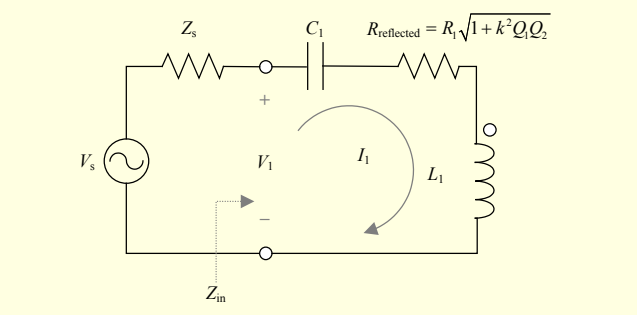

Fig. 2. Equivalent circuit model of two-coil WPT system with optimum load.

expressed as

$$Z_{\mathrm{in}}\big|_{Z_{\mathrm{L}} = Z_{\mathrm{L,opt}}} = R_1\sqrt{1 + k^2 Q_1 Q_2} + \mathrm{j}\omega L_1 + \frac{1}{\mathrm{j}\omega C_1}, \quad (21)$$

where the first term on the right-hand side is the resistance reflected by the secondary resonator. Using the reflected resistance, the two-coil WPT system of Fig. 1(a) with the optimum load can be represented simply, as shown in Fig. 2.

Because the ideal maximum PTE of (20) is derived from the operating power gain, it does not include the effect of the source impedance. In other words, the WPT system cannot achieve the maximum PTE of (20) even if the optimum load condition is satisfied. It is possible to maximize the PTE when the source delivers the maximum power to the network; that is, the source impedance has to conjugate-match the input impedance Z_{in}. Therefore, the optimum source condition is

$$Z_{\mathrm{s,opt}} = Z_{\mathrm{in}}^* = R_1\sqrt{1 + k^2 Q_1 Q_2} - \mathrm{j}\left(\omega L_1 - \frac{1}{\omega C_1}\right). \quad (22)$$

Inserting (22) and (1)–(3) into (6) gives

$$Z_{\mathrm{out}}\big|_{Z_{\mathrm{s}} = Z_{\mathrm{s,opt}}} = R_2\sqrt{1 + k^2 Q_1 Q_2} + \mathrm{j}\left(\omega L_2 - \frac{1}{\omega C_2}\right). \quad (23)$$

We are able to determine that the output impedance of (23) is conjugate-matched to the optimum load of (18) and (19), that is, $Z_{\mathrm{out}} = Z_{\mathrm{L,opt}}^*$. This means that the optimum source condition enables the output impedance to be conjugate-matched with the optimum load. Reciprocally, the optimum load also renders the input impedance conjugate-matched with the optimum source.

III. Matching-Network Topologies

A WPT system achieves the ideal maximum PTE when the optimum load and source conditions are satisfied. Matching networks of the WPT system transform the source and load impedances to the optimum ones.

Figure 3 shows a two-coil WPT system using input and

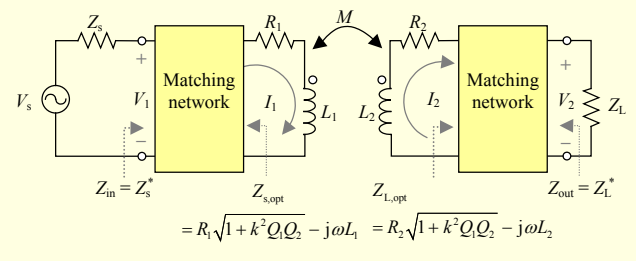

Fig. 3. Equivalent circuit model of two-coil WPT system using input and output matching networks under a maximum PTE.

output matching networks under a maximum PTE. The capacitors C_1 and C_2 of Fig. 1(a) are included in the matching networks, and are thus not shown in Fig. 3.

A matching network can be implemented in various forms such as that of a transformer, lumped elements, or transmission line. Because a matching network using transmission lines is only appropriate at a high frequency, such as the microwave frequencies, a general WPT system has difficulty using transmission lines. At a low frequency, lumped elements can be used to construct a matching network, which can result in various structures such as an L-section, π-section, and T-section. Figure 4(a) illustrates a typical two-coil WPT system used in an L-section lumped reactive matching network.

When the source impedance is transformed into the optimum source impedance by an input matching network, the secondary resonator with the output matching network and load can be represented using the reflected impedance, as shown in Fig. 4(b). The parallel and series capacitors, C_p and C_s, are tuned to match the load impedance with the reflected impedance, $Z_{reflected} = R_2\sqrt{1+k^2Q_1Q_2} + j\omega L_2$. We can evaluate the accurate parallel and series capacitances using analytic solutions of the L-section matching network in [21].

On the other hand, if the matching networks are implemented using an air-core transformer, which is a transformer without a magnetic core, a two-coil WPT system changes into the form of a general four-coil WPT system, as shown in Fig. 5. In other words, owing to the use of an air-core transformer, a two-coil WPT system can be converted into a four-coil WPT system.

In the case of $X_s + j\omega_0 L_s + 1/j\omega_0 C_s = 0$ and $X_L + j\omega_0 L_L + 1/j\omega_0 C_L = 0$, the typical four-coil WPT system in Fig. 5(a) is equivalent to the form of the two-coil WPT system in Fig. 5(b). In Fig. 5(b), when changing the distance and alignment between coils, we can control the mutual inductances, M_s and M_L, such that the reflected source and load impedances, $(\omega M_s)^2/(R_s + R_{ps})$ and $(\omega M_L)^2/(R_L + R_{pL})$, are matched to the optimum source and load resistance, $R_1\sqrt{1+k^2Q_1Q_2}$

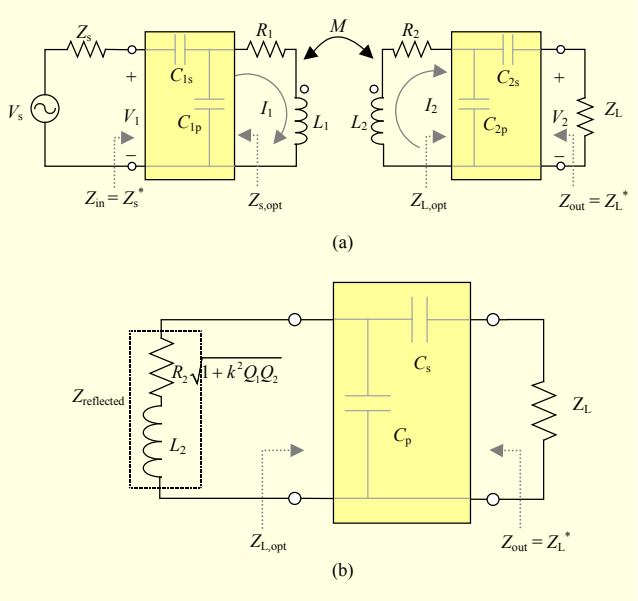

Fig. 4. Typical two-coil WPT system: (a) two-coil WPT system with L-section matching networks and (b) L-section matching arbitrary load impedance with reflected impedance.

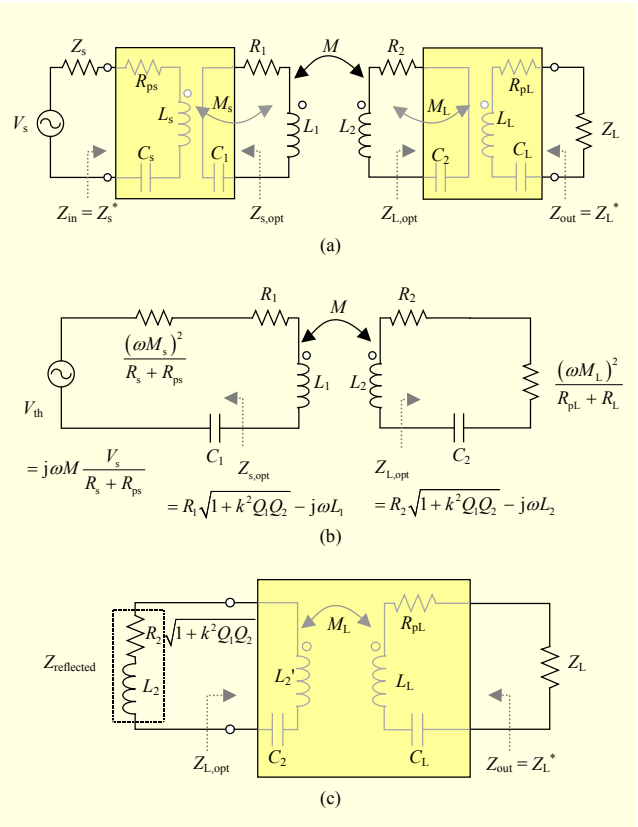

Fig. 5. Typical four-coil WPT system: (a) two-coil WPT system with air-core transformer matching networks, (b) equivalent circuit model at resonant frequency, and (c) air-core transformer matching arbitrary load impedance with reflected impedance.

and $R_2\sqrt{1+k^2Q_1Q_2}$. For the reactance part, the resonant capacitors, C_1 and C_2, are tuned to cancel the inductance of the coils and conjugate-match the primary and secondary coils to the optimum source and load conditions.

In the case of the four-coil WPT system, the secondary resonator is represented using the reflected impedance, as shown in Fig. 5(c). The primary and secondary coils are used to transfer power between coils, as well as to construct the matching networks. Because the reflected impedance includes the inductance of the secondary coil, L_2, the inductance of the matching network, L_2', should be modeled as 0 H. Therefore, the matching network circuit of Fig. 5(c) cannot be implemented using a real inductor, and can only be analyzed through a simulation.

IV. Simulation Results and Discussion

Thus far, our study has ascertained that two- and four-coil WPT systems are different only in terms of the structure of their input and output matching networks.

In this section, we analyze the characteristics of the L-section and air-core matching networks, and compare a two-coil WPT system with a four-coil WPT system in terms of efficiency. For the sake of the comparison, we used the Advanced Design System (ADS) of Keysight Technologies, which is one of the most powerful tools for an RF design and simulation, and the High Frequency Structural Simulator (HFSS) of ANSYS, which is a 3D EM simulator based on a finite element method.

The parameters for the system used in this simulation, as shown in Fig. 1(a), are described in Table 1. We use the same parameter values as used in [3], which were designed to achieve the maximum PTE at the target coupling coefficients. For the strongly and weakly coupled cases, the target coupling coefficients are set to 0.0125 and 0.005, respectively. The unloaded Q-factor of each coil is 1,256.5 at an operating frequency of 10 MHz, and the FoMs of the strongly and weakly coupled cases, $\Delta = k^2Q_1Q_2$, are 246.74 and 39.48, respectively. From (20), the ideal maximum PTEs of the strongly and weakly coupled cases are 0.8805 and 0.7283, respectively.

1. Characteristics of Matching Networks

To achieve these maximum PTEs, the optimum load and source conditions of (18), (19), and (22) should be satisfied. As mentioned before, for simplicity of the circuit, suppose the capacitors of (18) and (21)–(23), C_1 and C_2, are included in the matching networks. In the strongly coupled case, both the optimum source and load impedances, $Z_{s,opt}$ and $Z_{L,opt}$, become

Table 1. Circuit values used to evaluate simplified model.

Parameters	Value	Description
L_1, L_2	20 μH	Inductance of primary and secondary coil
R_1, R_2	1 Ω	Parasitic resistance of primary and secondary coil
Z_s, Z_L	50 Ω	Source and load impedances
k	0.0125	Coupling coefficient of strong-coupled case
	0.0050	Coupling coefficient of weak-coupled case
f_0	10 MHz	Operating frequency

Table 2. Evaluated parameter values of matching networks.

	Parameters	Values	
		Strong coupling (k = 0.0125)	Weak coupling (k = 0.005)
L-section matching network	C_{1s}, C_{2s}	7.11 pF	4.52 pF
	C_{1p}, C_{2p}	5.56 pF	8.15 pF
Air-core transformer matching network	L_s, L_L	1 μH	
	R_{ps}, R_{pL}	0.25 Ω	
	C_1, C_2	12.67 pF	
	C_s, C_L	253.3 pF	
	M_s, M_L	447.6 nH	284.6 nH
	k_s, k_L	0.1001	0.0636

15.74 – j1256.6 Ω. For the weakly coupled case, both $Z_{s,opt}$ and $Z_{L,opt}$ become 6.36 – j1256.6 Ω. The matching networks used to transform the source and load impedances into $Z_{s,opt}$ and $Z_{L,opt}$ can be configured using the L-section and air-core transformer, as shown in Figs. 4(b) and 5(c). Therefore, with the S-parameter simulation controller of the ADS, we simulate the circuits of Figs. 4(b) and 5(c), each of which consists of two-port impedance terminations and lumped elements. The used capacitors are modeled with an ideal capacitor and a small resistor in series having an equivalent series resistance (ESR) of 0.0015 Ω (for authenticity).

For the strongly and weakly coupled cases, the parameters for the matching networks are evaluated. The evaluated parameter values are shown in Table 2, where it can be seen that the values in the case of the strongly coupled four-coil WPT system are identical to those used in [3].

To investigate the characteristics of the matching networks, the matching networks of the L-section and air-core transformer are constructed using the parameter values in Table 2 for the strongly coupled two-coil and four-coil WPT systems. Figure 6 shows the reflection and transmission coefficients as well as the input and output impedances versus the frequency. No noticeable differences in bandwidth are

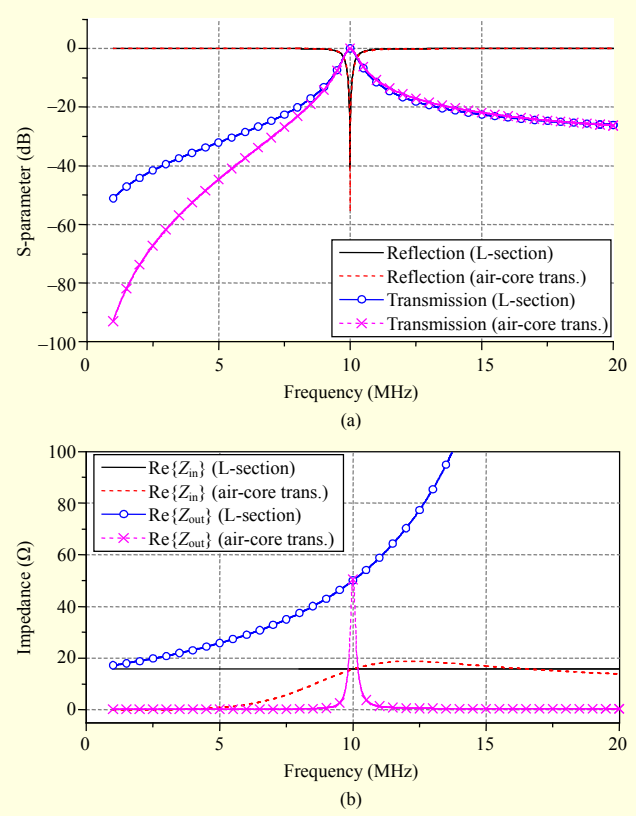

Fig. 6. Frequency characteristics of matching networks for strongly coupled WPT system: (a) reflection and transmission coefficients, and (b) input and output impedances.

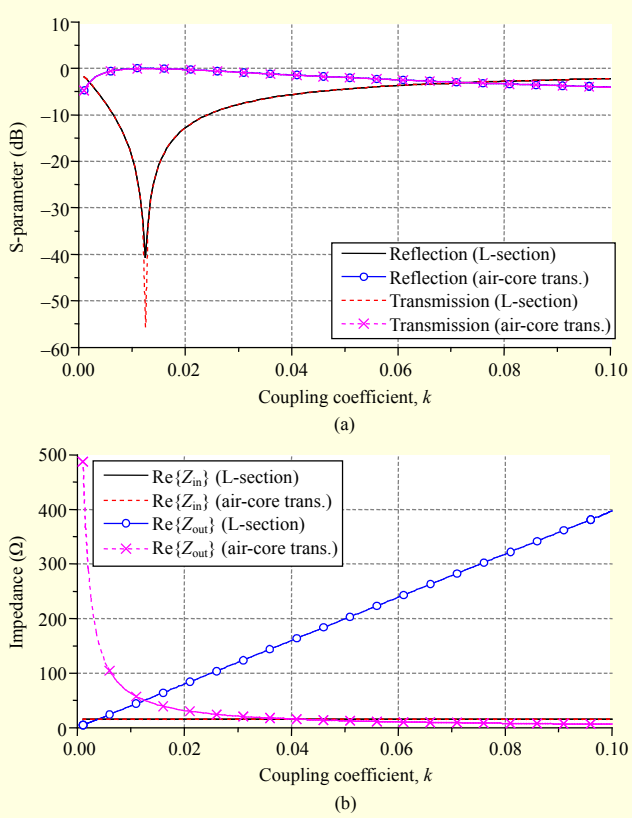

Fig. 7. Characteristics of matching networks at operating frequency of 10 MHz with respect to coupling coefficient between primary and secondary coils for strongly coupled WPT system: (a) reflection and transmission coefficients and (b) input and output impedances.

observed for the two matching networks. Moreover, at an operating frequency of 10 MHz, the two matching networks have similar reflection and transmission characteristics. The reflection coefficient of the air-core transformer is about −55 dB at the operating frequency of 10 MHz, while that of the L-section is about −40 dB. The reflection coefficient difference of 15 dB between the two matching networks means that the performance of a matching network that uses an air-core transformer is better than that using reactive lumped elements. In particular, the reflection coefficients are less than −40 dB and the transmission coefficients are nearly 0 dB, which means that most of the power into the matching networks is transferred to the load. That is, a reflection coefficient of less than −40 dB and a transmission coefficient of nearly 0 dB is enough to claim that the efficiency of a WPT system is going to be slightly affected. In addition, the two matching networks have the same input resistance of 15.7 Ω, which is identical to that of the optimum load, and the output impedance also becomes a load impedance of 50 Ω. However, the input and output impedances of the two matching networks have substantially different frequency characteristics except at around 10 MHz.

Figure 7 shows the S-parameters and impedance with respect to the coupling coefficient between the primary and secondary coils for the two types of matching networks. When the coupling coefficient varies from 0.001 to 0.1, the L-section and air-core transformer matching networks have the same transmission and reflection coefficients. The transmission coefficient is nearly 0 dB, and the reflection coefficient is less than −40 dB at a target coupling coefficient of 0.0125. On the other hand, the input impedances of the two matching networks remain unchanged, because the output port impedance (that is, the load impedance) is not a function of the coupling coefficient, k.

On the contrary, the input port impedance, $Z_{reflected}$, increases with the coupling coefficient, as shown in Figs. 4(b) and 5(c). Hence, the output impedances of the two matching networks change with respect to the coupling coefficient, but have a different trend of variation. The output impedance of the L-section increases with the coupling coefficient, whereas that of the air-core transformer decreases with the coupling coefficient. However, at the target coupling coefficient (k =

0.0125), the output impedance of the two matching networks has the same value of 50 Ω, which is the value of the load impedance. It is notable that both types of matching network have different impedance characteristics, with the exception of the target coupling coefficient and operating frequency, but have nearly identical S-parameter characteristics.

2. Efficiencies of Two- and Four-Coil WPT Systems

We compare the two-coil WPT system with the four-coil WPT system in terms of transmission coefficient and efficiency, such as operating and transducer power gains.

The operating power gain, G_p, represents the relation between a two-port network and the load impedance. Therefore, after the source part is directly connected to the two-port network by eliminating the input matching network shown in Fig. 3, the operating power gain of (9) is estimated with the Z-parameters, whereas the transducer power gain is obtained using the Z-parameters simulated with the input and output matching networks. To obtain the Z-parameters, we simulate the circuits of Figs. 4(a) and 5(a) using the S-parameter simulation controller of the ADS. However, for the S-parameter simulation, the voltage source and source impedance are replaced with a port impedance terminator having an identical source impedance. Similarly, the load impedance is replaced with a port impedance terminator having an identical load impedance. Additionally, the four-coil WPT system of Fig. 8 is simulated using the EM solver of ANSYS HFSS. For the two-coil WPT system, the primary and secondary coils of Fig. 8 are only simulated without the source and load coils. The lumped RLCs are used to resonate at the operating frequency.

Figure 9 shows the efficiencies of a strongly coupled case (k = 0.0125) using (9) and (14) as a function of the coupling coefficient between the primary and secondary coils. The EM-simulated results show good agreement with the circuit-simulated ones. Both the two- and four-coil WPT systems have similar efficiencies for the operating and transducer power gains. The efficiencies of the four-coil WPT system are slightly less than those of the two-coil WPT system, which results from the fact that the air-core transformers used in the four-coil WPT system have parasitic resistances, R_{sL} and R_{pL}. That is, the air-core transformers are a lossy matching network, whereas the L-section matching network in the two-coil WPT system uses only reactive elements. In most cases, because the parasitic resistances of the source and load coils are smaller than the source and load impedances, their effect on the PTE may be negligible. The transducer power gains of the two-coil and four-coil WPT systems reach an ideal PTE of 88% at k = 0.0125. The deviation of the coupling coefficient from the

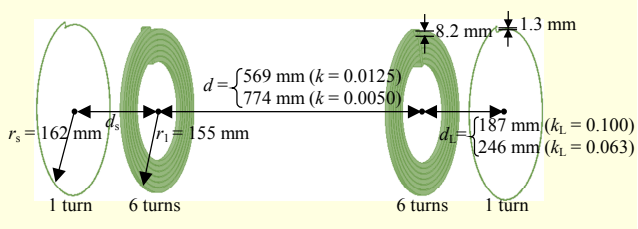

Fig. 8. Geometry of four-coil WPT system for 3D EM simulation.

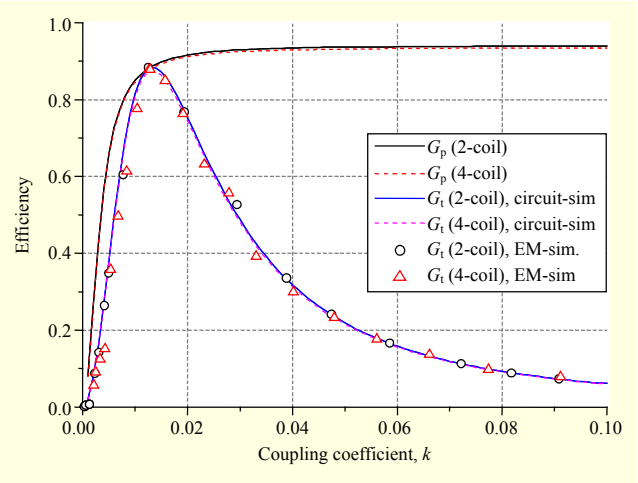

Fig. 9. Operating and transducer power gains of strongly coupled two- and four-coil WPT systems at operating frequency of 10 MHz with respect to coupling coefficient.

target coupling coefficient brings about a decrease in the PTE. The high value of PTE at around the target coupling coefficient results from the steep reflection characteristics of the matching networks, as shown in Fig. 7(a). These phenomena can be explained by the frequency splitting.

Figure 10 shows the transmission coefficients when the source and load impedances of the two-coil WPT system are replaced with the port. It should be noted that a frequency splitting appears at k > 0.0125. If the coupling coefficient exceeds the target coupling coefficient, then the input power of the WPT system is delivered to the load through the split frequencies, and not through the operating frequency. Therefore, the PTE at the operating frequency drops when k > 0.0125.

Under the assumption that the load impedance is transformed to the optimum load at k = 0.0125, the operating power gains are estimated as shown in Fig. 8. Contrary to the transducer power gain, the operating power gain increases as the coupling coefficient increases. This phenomenon indicates that although the optimal load of the target coupling coefficient is implemented, a high efficiency can be achieved by adjusting only the source part beyond the target coupling coefficient.

The operating and transducer power gains versus the load

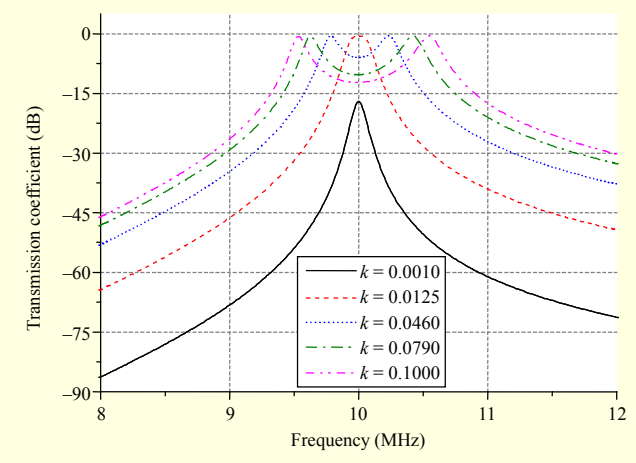

Fig. 10. Transmission coefficients of strongly coupled two-port WPT system as function of frequency for several coupling coefficients.

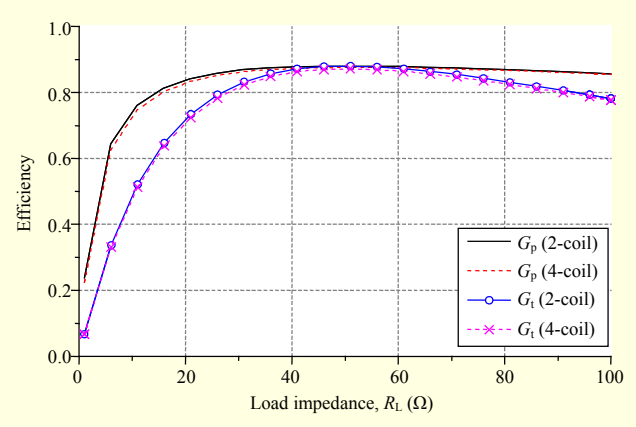

Fig. 11. Operating and transducer power gains of strongly coupled two- and four-coil WPT systems at operating frequency of 10 MHz with respect to load impedance.

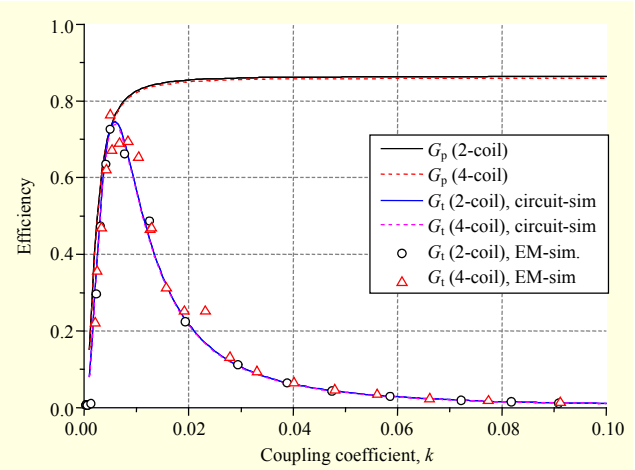

Fig. 12. Operating power gain and transducer power gain of weakly coupled two- and four-coil WPT systems at operating frequency of 10 MHz with respect to coupling coefficient.

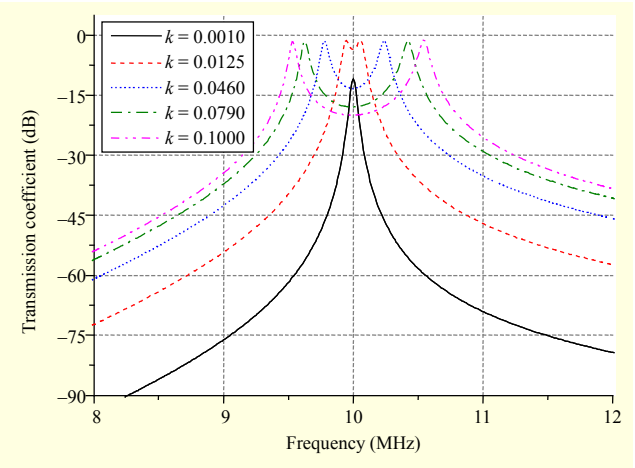

Fig. 13. Transmission coefficients of weakly coupled two-port WPT system as function of frequency for several coupling coefficients.

impedance in the cases of the two- and four-coil WPT systems are plotted in Fig. 11. The efficiencies of the two- and four-coil systems are also alike. The parameters in Table 2 were calculated for the maximum PTE at a load impedance of 50 Ω.

Figure 12 shows the operating and transducer power gains for the weakly coupled two- and four-coil WPT systems, which were designed to achieve the maximum PTE at a coupling coefficient of 0.005. Similarly to the strongly coupled WPT systems, the operating power gain of the weakly coupled WPT systems increases as the coupling coefficient increases. In addition, the operating and transducer power gains of the two- and four-coil WPT systems look almost identical. The two WPT systems show the same performance when designed for the same target coupling coefficient and operating frequency. The results of the circuit simulation are in agreement with those of the EM-simulation. The only difference between the two WPT systems can be found in the structures of their respective matching networks.

At a target coupling coefficient of 0.005, the transducer power gains of the two- and four-coil WPT systems are maximized to 72%, which is identical to the ideal PTE. Beyond the target coupling coefficient, the operating power gain drops sharply as in the strongly coupled case. In the strongly coupled case shown in Fig. 10, the maximum frequency is split into two maxima when $k > 0.0125$. In contrast, the weakly coupled case in Fig. 13 already has two maximum frequencies when $k = 0.0125$. Therefore, the frequency splitting occurrence depends on the source and load impedances. The optimum source and load conditions maximize the transmission coefficient at the operating frequency without splitting the frequency. A critical coupling occurs when the highest level of coupling is achieved without a

frequency splitting [3], [8]. Therefore, the optimum source and load conditions are identical to the critical coupling conditions.

The maximum operating power gain of the strongly coupled WPT system is about 0.94, as shown in Fig. 9, whereas that of the weakly coupled WPT system is 0.86, as shown in Fig. 12. In other words, according to the specific target coupling coefficient, the WPT system has a different maximum achievable efficiency.

V. Conclusion

We presented the operating power gain and transducer power gain of a two-coil WPT system using the Z-parameters, and derived the optimum load condition to maximize the operating power gain. Similarly, the optimum source condition was also derived. These optimum source and load conditions maximize the PTE of a two-coil WPT system.

We ascertained that the two- and four-coil WPT systems have the same efficiency for the same target coupling coefficient and operating frequency, with the two systems having only different matching networks; the two-coil WPT system has L-section (or lump-reactive) matching networks, whereas the four-coil WPT system has air-core matching networks. In particular, we presented how to determine the coupling coefficient to maximize the PTE of the four-coil WPT system. Therefore, our study provides analytical solutions regarding the easy design of a four-coil WPT system.

For the strongly and weakly coupled cases, two- and four-coil WPT systems were designed and simulated using ADS and HFSS software. The two cases had the same maximum PTE at the given target coupling coefficients. These results confirm the notion that two- and four-coil WPT systems can be regarded as similar from the point of view of circuitry. Additionally, we revealed the optimum source and load conditions that force a WPT system to reach a critical coupled state.

References

[1] A. Kurs et al., "Wireless Power Transfer via Strongly Coupled Magnetic Resonance," *Sci*., vol. 317, no. 5834, 2007, pp. 83–86.

[2] A. Karalis, J.D. Joannopoulos, and M. Soljačić, "Efficient Wireless Non-radiative Mid-range Energy Transfer," *Ann. Physics*, vol. 323, no. 1, Jan. 2008, pp. 34–48.

[3] A.P. Sample, D.T. Meyer, and J.R. Smith, "Analysis, Experimental Results, and Range Adaption of Magnetically Coupled Resonators for Wireless Power Transfer," *IEEE Trans. Ind. Electron*., vol. 58, no. 2, Feb. 2011, pp. 544–554.

[4] S. Cheon et al., "Circuit-Model-Based Analysis of a Wireless Energy-Transfer System via Coupled Magnetic Resonances," *IEEE Trans. Ind. Electron*., vol. 58, no. 7, July 2011, pp. 2906–2914.

[5] S. Cheon et al., "Wireless Energy Transfer System with Multiple Coils via Coupled Magnetic Resonances," *ETRI J*., vol. 34, no. 4, Aug. 2012, pp. 527–535.

[6] K. Lee and D.-H. Cho, "Diversity Analysis of Multiple Transmitters in Wireless Power Transfer System," *IEEE Trans. Magn*., vol. 49, no. 6, June 2013, pp. 2946–2952.

[7] K. Lee and D.-H. Cho, "Simultaneous Information and Power Transfer Using Magnetic Resonance," *ETRI J*., vol. 36, no. 5, Oct. 2014, pp. 808–818.

[8] D.-W. Seo, J.-H. Lee, and H.-S. Lee, "Optimal Coupling to Achieve Maximum Output Power in a WPT System," *IEEE Trans. Power Electron*., vol. 31, no. 6, June 2016, pp. 3994–3998.

[9] J. Lee and S. Nam, "Fundamental Aspects of Near-field Coupling Small Antennas for Wireless Power Transfer," *IEEE Trans. Antennas Propag*., vol. 58, no. 11, Nov. 2010, pp. 3442–3449.

[10] J.C. Schuder, J.H. Gold, and H.E. Stephenson, "An Inductively Coupled RF System for the Transmission of 1 kW of Power through the Skin," *IEEE Trans. Biomedical Eng*., vol. BME-18, no. 4, July 1971, pp. 265–273.

[11] W.H. Ko, S.P. Liang, and C.D.F. Fung, "Design of Radio-Frequency Powered Coils for Implant Instruments," *Medical Biological Eng. Comput*., vol. 15, no. 6, Nov. 1977, pp. 634–640.

[12] N. de N. Donaldson and T.A. Perkins, "Analysis of Resonant Coupled Coils in the Radio Frequency Transcutaneous Links," *Medical Biological Eng. Comput*., vol. 21, no. 5, Sept. 1983, pp. 612–627.

[13] C.M. Zierhofer and E.S. Hochmair, "High-Efficiency Coupling-Insensitive Transcutaneous Power and Data Transmission via an Inductive Link," *IEEE Trans. Biomed. Eng*., vol. 37, no. 7, July 1990, pp. 716–722.

[14] M. Kiani, U.M. Jow, and M. Ghovanloo, "Design and Optimization of a 3-Coil Inductive Link for Efficient Wireless Power Transmission," *IEEE Trans. Biomedi. Circuit Syst*., vol. 5, no. 6, Dec. 2011, pp. 579–591.

[15] M. Kiani and M. Ghovanloo, "A Figure-of-Merit for Designing High Performance Inductive Power Transmission Link," *IEEE Trans. Ind. Electron*., vol. 60, no. 11, Nov. 2013, pp. 5292–5305.

[16] R. Huang and B. Zhang, "Frequency, Impedance Characteristics and HF Converters of Two-Coil and Four-Coil Wireless Power Transfer," *IEEE J. Emerging Sel. Topics Power Electron*., vol. 3, no. 1, Mar. 2015, pp. 177–183.

[17] C.-J. Chen et al., "A Study of Loosely Coupled Coils for Wireless Power Transfer," *IEEE Trans. Circuits Syst. II: Express Briefs*, vol. 57, no. 7, July 2010, pp. 536–540.

[18] M. Kesler, *Highly Resonant Wireless Power Transfer: Safe, Efficient, and Over Distance*, WiTricity Corporation, 2013, Accessed Apr. 25, 2016. http://witricity.com/assets/highly-resonant-power-transfer-kesler-witricity-2013.pdf

[19] J. Kim et al., "Coil Design and Shielding Methods for a Magnetic Resonant Wireless Power Transfer System," *Proc. IEEE*, vol. 101, no. 6, June 2013, pp. 1332–1342.
[20] J. Kim and J. Jeong, "Range-Adaptive Wireless Power Transfer Using Multi-loop and Tunable Matching Techniques," *IEEE Trans. Ind. Electron.*, vol. 62, no. 10, Oct. 2015, pp. 6233–6241.
[21] D.M. Pozar, "*Microwave Engineering*," John Wiley & Sons, NY, USA, 2012, pp. 234–244.
[22] D. Ahn, M. Kiani, and M. Ghovanloo, "Enhanced Wireless Power Transmission Using Strong Paramagnetic Response," *IEEE Trans. Magn.*, vol. 50, no. 3, Mar. 2014, pp. 96–103.
[23] M. Ettorre and A. Grbic, "A Transponder-Based, Non-radiative Wireless Power Transfer," *IEEE Antennas Wireless Propag. Lett.*, vol. 11, Sept. 2012, pp. 1150–1153.
[24] M. Pinuela et al., "Maximizing DC-to-Load Efficiency for Inductive Power Transfer," *IEEE Trans. Power Electron.*, vol. 28, no. 5, Aug. 2012, pp. 2437–2447.

Dong-Wook Seo received his BS degree in electrical engineering from Kyungpook National University, Daegu, Rep. of Korea, in 2003 and his MS and PhD degrees in electrical engineering from the Korea Advanced Institute of Science and Technology, Daejon, Rep. of Korea, in 2005 and 2011, respectively. He was a senior researcher for the Defense Agency for Technology and Quality, Daegu, Rep. of Korea, from 2011 to 2012. Since 2012, he has been a senior researcher at ETRI, Daegu, Rep. of Korea. His current research interests include numerical techniques in the areas of electromagnetics, radar cross-section analysis, wireless power transfer, biomedical implantable devices, and automotive radar systems.

Jae-Ho Lee received his BS degree in electronic and electrical engineering from Kyungpook National University, Daegu, Rep. of Korea, in 2002 and his MS degree in electrical and electronic engineering from the Korea Advanced Institute of Science and Technology, Daejon, Rep. of Korea, in 2004. He was awarded his PhD in electrical and electronic engineering from the Tokyo Institute of Technology, Japan, in 2010. From 2004 to 2005, he worked for the Mobile Communication PM Team, Institute of Information and Technology Assessment, Daejeon, Rep. of Korea. He also worked for the Radar Research Center, Samsung Thales, Yongin, Rep. of Korea, from 2010 to 2012. Since 2013, he has been a senior researcher at ETRI, Daegu, Rep. of Korea. His research interests include waveguide arrays, electromagnetic numerical analysis, biomedical implantable devices, automotive radar systems, and antennas.

Hyung Soo Lee received his BS degree in electrical engineering from Kyungpook National University, Daegu, Rep. of Korea, in 1980 and his PhD in IT engineering from Sungkyunkwan University, Suwon, Rep. of Korea, in 1996. Since 1983, he has been a principal researcher at ETRI, Daejeon and Daegu, Rep. of Korea. His research interests in clued spectrum engineering, WPAN system design, and biomedical IT convergence devices.